Vol.67: e24230703, 2024
https://doi.org/10.1590/1678-4324-2024230703
ISSN 1678-4324 Online Edition

BABT
Brazilian Archives of Biology and Technology

Article - Engineering, Technology and Techniques

MRI Imaging Techniques and Artificial Ligaments for the Diagnosis and Reconstruction of Cruciate Ligament Injuries of the Knee Joint

Jiebing Li [1*]
https://orcid.org/0009-0005-1614-8581

[1]Shijiazhuang people's Hospital, Bone and Joint Department, Shijiazhuang, Hebei, China.

Editor-in-Chief: Alexandre Rasi Aoki
Associate Editor: Raja Soosaimarian Peter Raj

Received: 08-Jul-2023; Accepted: 15-Apr-2024.

*Correspondence: jiebingli5@gmail.com(J.L.).

HIGHLIGHTS

- Structural problems within the isolated ligament were detected
- Satin Bowerbird Optimizer (SBO) method for accelerating the performance of the model.
- CL injury diagnosis system's area under the ROC curve was 98.5.

Abstract: This study focused on the use of MRI imaging techniques and artificial ligaments in diagnosing and reconstructing Cruciate Ligament (CL) injuries of the knee joint. CL injuries are common in athletes and can cause significant pain and disability. MRI imaging is a powerful diagnostic tool that accurately identifies the extent and location of the injury. The use of Artificial ligaments has been increasing in the surgical reconstruction of the ligament. In this study, we offer a deep learning (DL)-a based method called ThreeFold CNN for arthroscopically detecting injuries to the CL in the knee during MRI. The CL on MRI was first separated using two deep convolutional neural networks (2DCNNs). Then structural problems within the isolated ligament were detected using a classification CNN to create a completely automated DL-based diagnostic method. We employ the Satin Bowerbird Optimizer (SBO) method for accelerating the performance of the model. The CL injury diagnosis system's specificity and sensitivity are 97 and 97, respectively, at the optimum threshold. In contrast, the clinical radiologists' specificity varied between 0.91 and 0.99, while their sensitivity was between 0.97 and 0.99. The diagnostic performance of the CL injury diagnosis system and CR did not differ in a statistically significant manner at$P < .05$. The CL injury diagnosis system's area under the ROC curve was 98.5, which indicates outstanding overall diagnostic accuracy.

Keywords: Cruciate ligament (CL); MRI; artificial ligaments; injury diagnosis.

INTRODUCTION

Cruciate ligament injuries are common in athletes and can result in significant pain and disability. The knee joint is particularly susceptible to such injuries due to the complex biomechanics involved in its movement [1]. Both the anterior cruciate ligament (ACL) and the posterior cruciate ligament (PCL) perform essential functions in maintaining the condition and performance of the knee joint. The collateral ligament (CL) is a prevalent location for injury in athletes, and such damages can have spanning effects on an

individual's ability to engage in activities or other external operations [2-3]. Knee ligament (CL) injuries are depicted conceptually in Figure 1.

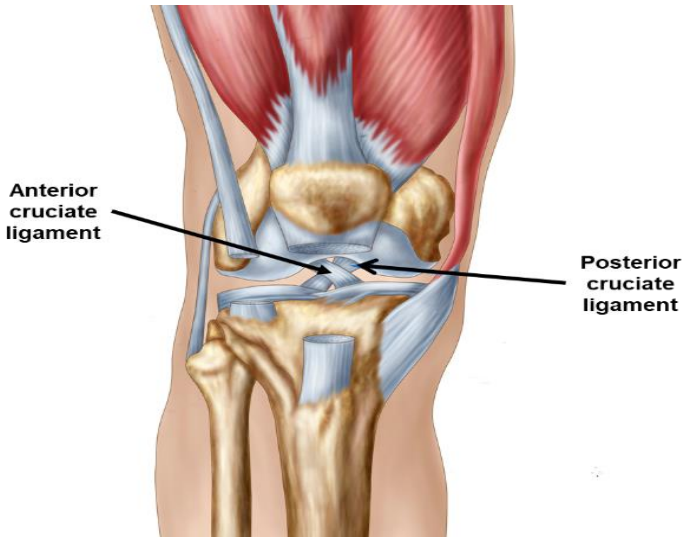

Figure 1. CL injuries of the knee joint

The diagnosis and treatment of cruciate ligament injuries have been greatly improved by advances in medical imaging and surgical techniques. MRI is a powerful diagnostic tool that allows for the accurate identification of the extent and location of the injury. MRI imaging techniques have greatly improved the diagnosis of cruciate ligament injuries and have helped to guide the development of more effective treatment options [4].

Surgical reconstruction of the cruciate ligament is often required to restore the stability and function of the knee joint [5]. Artificial ligaments have been developed to replace the damaged ligament and provide support to the knee joint during the healing process. The use of artificial ligaments has been shown to improve the outcomes of patients undergoing cruciate ligament reconstruction surgery. However, MRI is a commonly used imaging modality for the diagnosis of CL injuries, accurate diagnosis and diagnosis of these injuries can be challenging and require expertise [6].

In this study, we propose a DL-based method for arthroscopically detecting injuries to the CL in the knee during MRI. The proposed method involves using a two-stage DL approach. Firstly, a ThreeFoldCNNis used to isolate the CL from the MRI image. This is followed by the diagnosis of structural anomalies within the isolated CL using a categorization CNN in a DL-based diagnosis system.

This study aims to develop a reliable and accurate automated system for detecting CL injuries on MRI, which can assist radiologists and clinicians in making accurate diagnoses. The proposed DL-based method has the potential to improve the accuracy and efficiency of CL injury diagnosis on MRI, leading to earlier diagnosis and improved patient outcomes.

Contribution

This research effectively combines sophisticated MRI imaging methods with artificial ligaments, offering an integrated approach to the diagnosis and reconstruction of CL damage in the knee joint.

We present a new ThreeFold CNN approach for arthroscopic identification of CL injuries in MRI scans, demonstrating the capability of deep learning in automating diagnostic procedures to achieve efficient and precise outcomes.

The use of 2DCNNs for accurate differentiation and isolation of the CL on MRI demonstrates the effectiveness of deep learning in image segmentation, an essential stage in the diagnostic process.

The integration of the Satin Bowerbird Optimizer approach enhances the speed of the deep learning model, emphasizing the significance of optimization techniques in improving the effectiveness of diagnostic systems for CL injuries when compared to conventional clinical radiology approaches.

RELATED WORKS

Study [7] employed the 3D-CT technique to recreate the ACL's natural femoral impression and double-bone tract. To aid in the development of anatomic double-beam repair of the ACL by arthroscopy, they compare the positions of the two centers and outline the law governing their interaction. According to the

findings of the 3D reconstruction, the thickness of the UF layer forms a peak in the front, medial region and afterward diminishes in the posterior medial regions.

Research [8] shows that it was possible to train a DL CNN algorithm to detect the existence of a full ACL injury with an accuracy of over 96% on a test set. In addition, they investigate a variety of network designs tailored to the specific difficulties inherent in MRI-based sports injury diagnosis. They first show that the intercondylar area is where the input field of view has to be restricted to achieve optimal algorithm performance. Second, they show that the contextual information of neighboring imagine slices may significantly enhance the classification accuracy of a network.

Research [9] employed DL to improve the quality of Fourier approximation images, and it demonstrated the diagnostic value of a 5-minute 3D qDESS MRI sequence that yields multi-contrast images and concurrent quantitative T2 relaxation time observations. When arthroscopic results were employed as the supreme standard, the fast procedure exhibited good concordance with the imaging results from a typical diagnosis knee MRI protocol that required around 20 minutes.

To investigate the effectiveness of MRI based on DL in the diagnosis of ACL injury, a multimodal feature fusion DL model was created in the study [10] and used in the diagnosis of patients with ACL injuries. The outcomes demonstrated that DL-based MRI significantly enhanced the capacity to identify ACL injury and improved sensitivity, specificity, and accuracy.

The goal of the research [11] was to use a “semi-supervised framework, double-linear layers U-Net (DCLU-Net)” to create a DL model for segmenting and classifying MRI images of ACL injuries for diagnostic purposes. The goal of the study [12] was to determine if a 3D fat-suppressed proton density (FS-PD) multi-planar voxel picture of the knee was more beneficial than a thin-slice, high-resolution 2D FS-PD image utilizing a denoising technique using DL-based reconstruction (dDLR) with maximum-probability reconstruction (MPR).

In research [13], they apply and compare four different machine learning classification models to the well-balanced, structured ACL dataset: “the random forest (RF), the categorical boosting (Cat Boost), the light gradient boosting machines (LGBM), and the highly randomized classifier (ETC)."

Study [14] developed an “efficiently-layered network (ELNet)” CNN architecture on MRNet and validated it using MRI scans of knee ACL injuries. The model had a small number of parameters—about 0.2 million—and was lightweight. The study only gave AUC for the knee MRI dataset, which was a constraint in terms of accuracy because 90% was not an adequate result for tears in the ACL as assessed on MRNet.

Four classifications of ACL injuries were utilized in research [15] of hierarchical severity. Both the 2D and 3D CNN models were used to evaluate the CNN model. Although the 2D CNN performed better overall than the 3D CNN, it was poorer without transfer learning. Due to the small size of the test set, subcategories of partial tears could not be categorized, which was a drawback of the study. Radiologists determined the MRI ratings.

A study [16] uses a DL technique to automatically and effectively diagnose ACL tears. They created a DL model, which showed promise for patients with osteoarthritis and delivered the best performance for prospective classification. They offer cutting-edge research built on a customized CNN model following hyper-parameter adjustments. The outcomes showed that the CNN model built on DL significantly improved the categorization of knee ACL rupture.

ACL tears from magnetic resonance imaging were automatically segmented by DL in research [17]. With the help of the convolutional neural network architecture U-Net, a knee mask was created on the original MRIs. In study [18], 2D U-Net was utilized to partition the cartilage and meniscus into eleven groups. Using the same 3D U-Net CNN architecture technique, the meniscal cartilage and staging patellar boundary box severity were recognized in a cascade way.Research [19] suggested using a three-layered compressed parallel deep convolutional neural network to improve the attribute individuality of knee MRI data for detecting ACL splitting.

To improve injury detection algorithms' generalization capacity, a study [20-23] introduced a CNNs-based DL model, which achieved an accuracy of 87.5% on the MRNet dataset and 87.00% on the Knee MRI dataset. It has been found that DL frameworks can significantly outperform machine learning when it comes to detecting knee tears in MRI images. On the other hand, current knee injury detection designs employ complicated network structures, which increases the size of the training parameters.

Problem statement

The cruciate ligament of the knee is frequently injured, and artificial ligaments and MRI imaging methods are frequently used for diagnosis and treatment. These approaches do, however, face several difficulties that may compromise their precision and effectiveness. It can be difficult to get accurate images of the knee joint

using MRI imaging methods, especially if there is swelling or other tissue damage. This might make it challenging for medical professionals to appropriately assess the severity of the injury and choose the most appropriate course of action. The fact that MRI imaging may be costly and may not be reimbursed by all insurance plans presents another difficulty.As a result, some patients may find it challenging to get access to this crucial diagnostic tool. One issue with artificial ligaments is that they might not always be able to offer the same amount of support and stability as a natural ligament. This may result in issues with the artificial ligament's mobility and long-term durability. To address these problems, a ThreeFoldCNNwas used, and in a DL-based diagnosis system, a classification CNN was used to find structural defects inside the isolated CL. To improve the model's performance, we use the Satin Bowerbird Optimizer (SBO) technique.

METHODS

In this research, we provide a DL-based approach to CL injury diagnosis in the knee via MRI depicted in figure 2. In this article, we propose ThreeFoldCNN, which contains two deep convolutional neural networks (2DCNNs) for splitting CL on MRI, and then defects within the isolated ligament were discovered using a classification CNN. The ThreeFoldCNN deep learning model employs a triple convolutional neural network development to examine medical imaging data, which in consequence improves the accurate assessment and 3D regeneration of knee cruciate ligament damage. To improve the model's performance, we use the Satin Bowerbird Optimizer (SBO) technique A cruciate ligament injury to the knee can be diagnosed and reconstructed with the use of a natural-inspired algorithm called Satin Bird Optimization (SBO). It optimizes diagnostics and treatments by emulating the mating behaviors of satin bowerbirds.

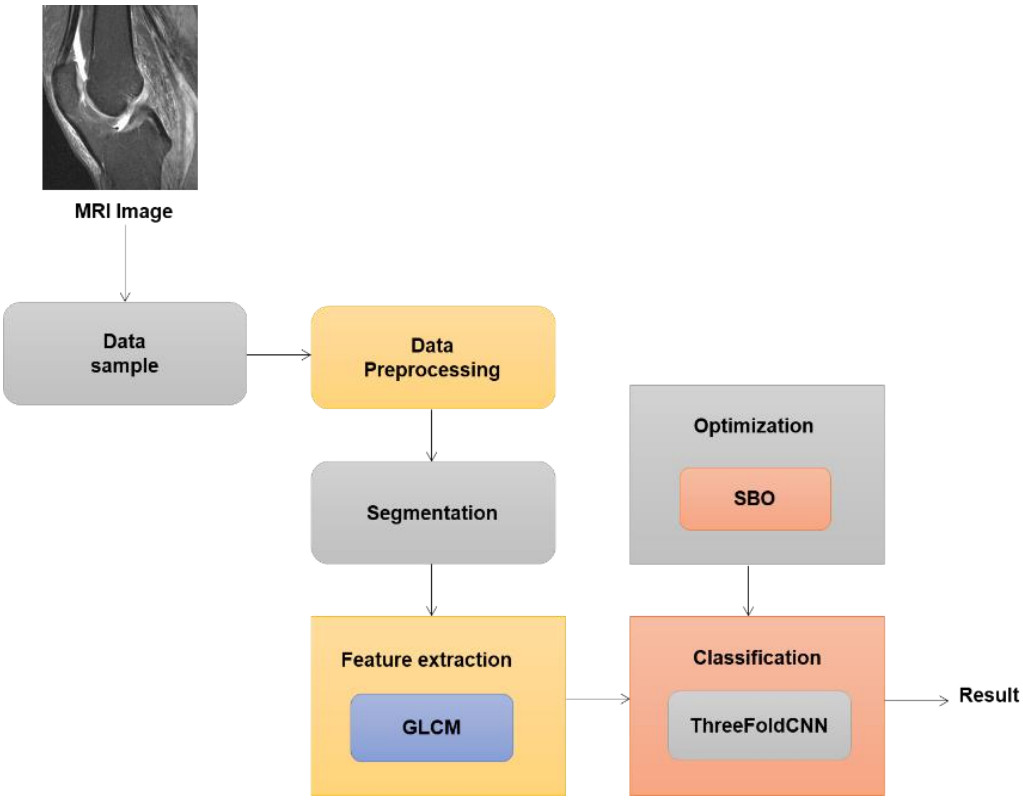

Figure 2. Outline of the suggested approach

Data sample

The provisions of the "Health Insurance Portability and Accountability Act" were followed in conducting the current retrospective investigation with the approval of our Chinese institutional review panel and without any requirement for informed consent to be obtained. One hundred seventy-seven people with a surgically verified injury to the CL [99 men, 78 women; mean age: 28.5 years, range of age: 17-48 yrs.] and 177 people with a surgically verified intact CL [101 men, 76 women; mean age: 40 years; the range of age: 18-52 years] had MRI data sets obtained. All MRI tests were conducted using the same 3 Tesla MRI scanner, as shown in Figure 3.

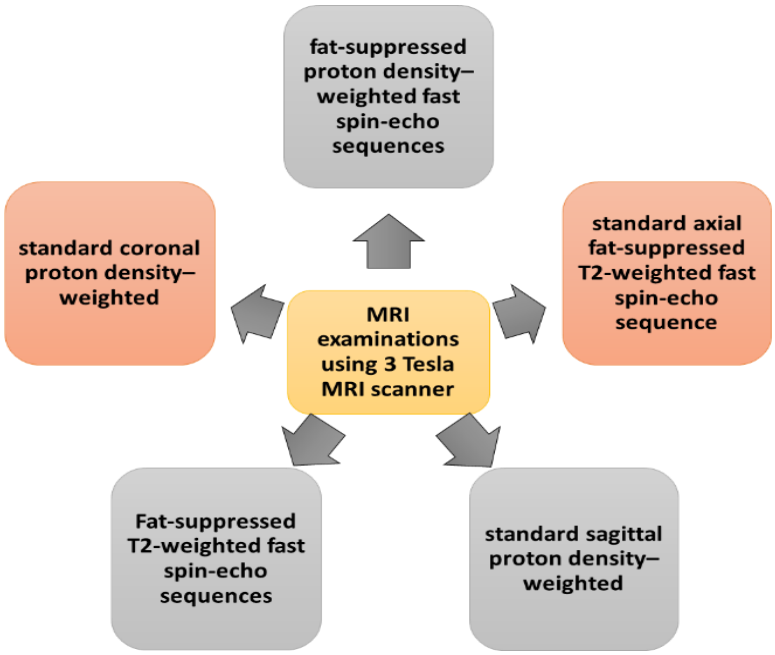

Figure 3. MRI evaluation using 3 Tesla MRI scanner

Table 1 summarizes the diagnostic parameters for the entire MRI testing sequences. A musculoskeletal radiologist (MR) with fifteen years of clinical expertise used a medical record-maintaining platform to randomly identify individuals with and without a CL injury. Patients scheduled for arthroscopic surgery on the knee at our hospital were checked to determine if they had recently undergone an MRI of their identical knee using the similar 3 Tesla MRI scanner within the four months before their surgery.

Table 1. MRI evaluation specifications for the scanning sequences

Parameter	Coronal Fat-Saturated Proton Density–weighted FSE	Sagittal Fat-Saturated T2-weighted FSE	Sagittal Proton Density–weighted FSE	Axial Fat-Saturated T2-weighted FSE	Coronal Proton Density–weighted FSE
Echo time (msec)	21	82	24	81	24
Flip angle (degrees)	90	90	90	90	90
Field of view (cm)	11	11	17	15	12
Repetition time (msec)	1820	5300	2500	4310	2100
Reconstruction matrix size	512 x 512	512 x 512	512 x 512	512 x 512	512 x 512
Acquisition matrix size	448 x 224	448 x 224	448 x 224	448 x 224	448 x 224
Section thickness (mm)	1	2	4	5	11
Echo train length	4	21	5	21	9
Field of view (cm)	14	14	11	18	11
Section thickness (mm)	2	5	2	4	2
Bit depth (bit)	16	16	16	16	16
Echo train length	4	20	4	21	4
Imaging time (min)	3:25	3:15	3:22	3:35	3:21

Data pre-processing

Image normalization is a process of rescaling the pixel intensity values of an image to a common range. MRI images of the knee joint may have varying intensity levels due to differences in scanner hardware and settings, which can affect the accuracy of subsequent analysis. Image normalization helps to ensure that the intensity levels of the image are consistent across different images. This can be done by subtracting the mean intensity value of the image and dividing it by the standard deviation or by scaling the pixel values to a common range, such as [0, 1] or [-1, 1].

Noise reduction is a process of removing unwanted noise from an image. MRI images of the knee joint may contain various types of noise, such as thermal noise and artifact noise, which can affect the accuracy of subsequent analysis. Noise reduction techniques such as smoothing filters can be used to remove noise from the image. One common technique is Gaussian smoothing, which involves convolving the image with a Gaussian kernel. This results in a blurred image that removes high-frequency noise.

Gaussian smoothing (GS) determines the gradient of a function by randomly selecting a direction from a traditional normal distribution, calculating the derivative of the function along that direction employing function assessments, and then multiplying the derivatives with the direction. Gaussian smoothing is a flexible zero-order strategy that may be easily incorporated into any gradient-based optimization technique by using the estimate.

The Gaussian smoothing gradient estimator is clearly defined in Equation (1),

$$\nabla_\theta E^{HT}(\theta)=\frac{1}{d}E(\theta+d\epsilon)\epsilon,\ \ \epsilon\sim N(0,J) \qquad (1)$$

It can be regarded as a Monte Carlo approximation of the gradient of the improved objective function, which has been smoothed using a typical normal random variable as shown in Equation (2).

$$E_d(\theta)\triangleq E_{\epsilon\sim N(0,J)}[E(\theta+d\epsilon)],\ \ d>0 \qquad (2)$$

The derivative of the improved objective function is provided by Equation (3),

$$\nabla_\theta E_d(\theta)= E_{\epsilon\sim N(0,J)}\left[\frac{1}{d}E(\theta+d\epsilon)\epsilon\right] \qquad (3)$$

Due to the frequent occurrence of significant variation in $\nabla_\theta E_d(\theta)$, often used alternatives are the forward-difference (FD) estimator and the antithetic (AT) estimator, both of which integrate control shifts for $\epsilon \sim \mathcal{N}(0,J)$, as shown in Equation (4),

$$\nabla_\theta E^{HT}(\theta)=\frac{1}{d}[E(\theta+d\epsilon)-E(\theta)]\epsilon \qquad (4)$$

$$\nabla_\theta E^{BS}(\theta)=\frac{1}{2c}[E(\theta+d\epsilon)-E(\theta-d\epsilon)]\epsilon \qquad (5)$$

Averaging over numerous directions helps decrease the variance of every estimator. We selected the FD estimator because of its simplicity and reduced computing load.

When $d \to 0$ demonstrates that iterative optimization employing gradients derived by Equation (5) converges to the optimal point for convex purposes and remains stationary for non-convex ones, and when $E(\theta)$ has some minor regularity requirements.

Segmentation

Image segmentation using thresholding is a common technique used in MRI image analysis of the knee joint for CL analysis. The threshold value should be chosen based on the expected intensity values of the foreground and background regions in the image. This can be done manually or using automated methods such as Otsu's thresholding or adaptive thresholding. The threshold value is applied to the image by comparing each pixel's intensity value to the threshold value.

Pixels with intensity values above the threshold are assigned to the foreground, while pixels with intensity values below the threshold are assigned to the background. The initial threshold-based segmentation may contain noise or errors, which can be refined using pre-processing techniques. Image segmentation using thresholding is a simple and effective technique for separating the CL from other structures in the knee joint

in MRI images. The CL typically has a distinct intensity range compared to other structures in the knee joint, making it suitable for segmentation using thresholding. However, this method may not be suitable for images with poor contrast or for detecting subtle changes in the CL structure.

Feature extraction

Grey level co-occurrence matrix (GLCM) is a widely used technique for feature extraction in image analysis, including MRI images of the knee joint for CL analysis. GLCM is a texture analysis method that quantifies the spatial relationship between pairs of pixels in an image by computing the frequency of occurrence of pairs of Grey-level values at a given offset and direction. The GLCM can be used to extract various texture-based features from the image, such as contrast, correlation, energy, and homogeneity. These features are based on the statistical properties of the GLCM and can provide information about the texture and structure of the image.

The extracted texture-based features can then be used as input to DL algorithms or other analysis techniques for CL analysis. GLCM is a powerful and widely used technique for feature extraction in MRI images of the knee joint for CL analysis. By quantifying the spatial relationships between pairs of pixels, GLCM can provide information about the texture and structure of the image, which can be useful for detecting subtle changes in the CL or other structures in the knee joint.

CL Injury Diagnosis System

When applied to medical imaging data, the deep learning model's triple convolutional neural network development generates more precise damage assessments and more effective 3D restoration of the knee cruciate ligament.

Three different CNNs (ThreeFoldCNN) made up the suggested DL-based CL injury diagnosis system. From the total MRI dataset, the initial CNN selected the CL-containing image segments. To limit the amount of information required for further image recognition, the subsequent CNN isolated an intercondylar notch (IN) portion, which included the CL on the selected image portions. In the third category, to determine whether a CL injury had occurred or not, CNN examined an individual CL on the selected imaging portions, a completely automated processing pathway was made by layering the ThreeFoldCNN.

Table 2 provides a summary of the CNNs' complex structure.

Table 2. Extensive System Architecture for the CL Isolation, Classification CNN, and Section-diagnosis

Section-diagnosis (1- CNN)	Classification (3- CNN)	CL Isolation (2- CNN)
Input (gray-scale image)	Input (gray-scale image)	Input (gray-scale image)
2DConv (6 7 x 7 filters), BN, ReLU	2DConv (32 7 x 7 filters)	2DConv (64 7 x 7 filters), BN, ReLU
MaxPool (window size 2 x 2)	MaxPool (window size 2 x 2)	MaxPool (window size 2 x 2)
MaxPool (window size 2 x 2)	2DConv (64 1 x 1 filters), BN, ReLU	MaxPool (window size 2 x 2)
FC (2 nodes)	Dense block: {2DConv (1 x 1 filters), BN, ReLU; 2DConv (3 x 3 filters), BN, ReLU} x 12	MaxPool (window size 2 x 2)
2DConv (16 5 x 5 filters), BN, ReLU	Dense block: {2DConv (1 x 1 filters), BN, ReLU; 2DConv (3 x 3 filters), BN, ReLU} x 6	2DConv (192 3 x 3 filters), BN, ReLU
		2DConv (128 1 x 1 filter), BN, ReLU
FC (84 nodes)	MaxPool (window size 2 x 2)	2DConv (256 3 x 3 filters), BN, ReLU 2DConv (256 1 x 1 filters), BN, ReLU 2DConv (512 3 x 3 filters), BN, ReLU
SoftMax (2 classes)	MaxPool (window size 2 x 2)	MaxPool (window size 2 x 2)
	Dense Block: {2DConv (1 x 1 filters), BN,	{2DConv (512 1 x 1 filters), BN, ReLU

Cont. Table 2

	ReLU; 2DConv (3 x 3 filters), BN, ReLU} x 24	2DConv (1024 3 x 3 filters), BN, ReLU}×2
		{2DConv (1024 3 x 3 filters), BN, ReLU}×4
	2DConv (128 1 x 1 filters), BN, ReLU	{2DConv (256 1 x 1 filters), BN, ReLU 2DConv (512 3 x 3 filters), BN, ReLU} x 4 2DConv (512 1 x 1 filters), BN, ReLU 2DConv (1024 3 x 3 filters), BN, ReLU
	SoftMax (2 classes)	Tensor (7 x 7 x 11)
	GlobalAveragePool	FC (4096 nodes)

The first part LeNet-5, which was initially developed to perform biological imagery analysis but has lately been employed for other medical imaging uses, served as the foundation for CNN. A CNN with two distinct sets of convolutional layers (CLs), and softmax classifier, and two fully linked layers, is depicted at the top of Figure 4.

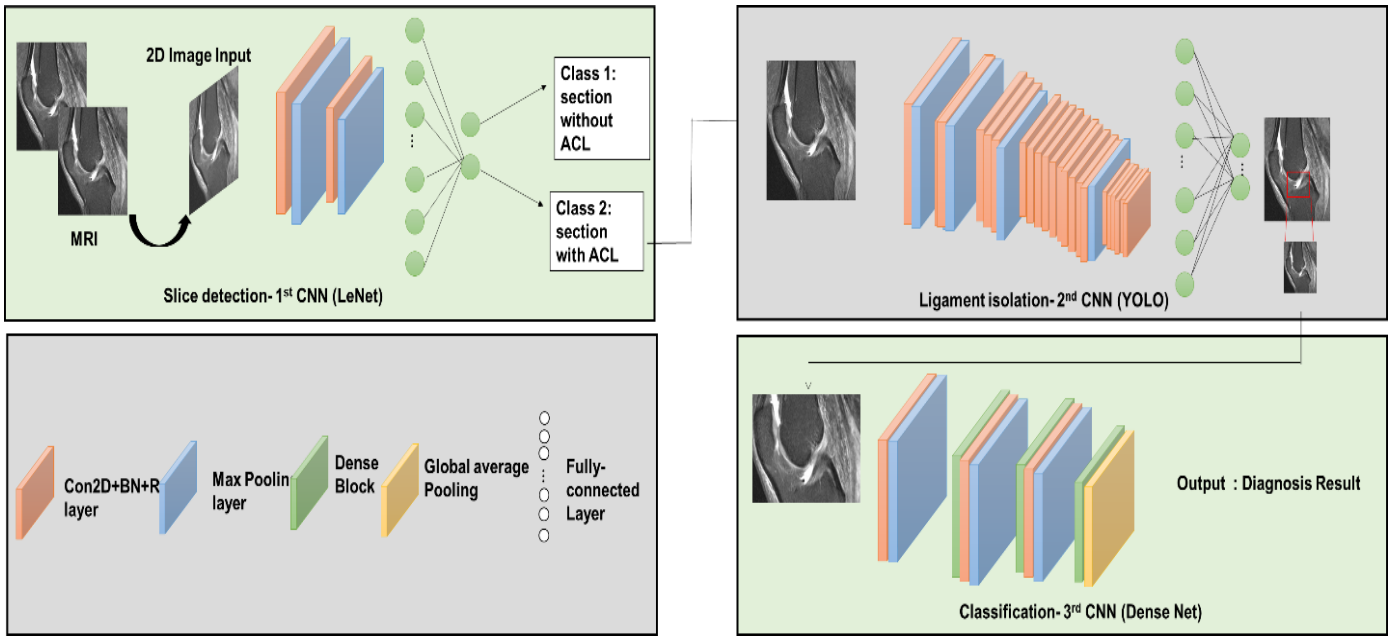

Figure 4. CL injury diagnosis system using ThreeFoldCNN

The CNN was altered to accommodate input images up to 448×448 with a range of 0 to 1 about the maximal MRI. One outcome class was designated for image segments with the CL, whereas the further was designated for image areas without the ACL. The second isolation of a ligament, "You Only Look Once, or YOLO," which was successful in several visual identification tests, served as an idea for CNN. A CNN with 24 CLs and two entirely linked layers is seen in the center of Figure 1. The CLs were applied to the particular image areas that included the CL to gather relevant image features.

A rectangular box, the dimensions of which were anticipated by the fully connected layers using the acquired image data, was used to describe the IN, which contained the CL. Images of the present attached in a "rectangle box," including the CL on the selected image regions, were utilized as the input images for the classification process using CNN and downscaled to112×112. CNN was inspired by a category of neural networks called "densely connected convolutional networks" that performed exceptionally well in an image recognition task using data from the Large Scale Visual Identification Challenge.

The three-fold dense blocks in this CNN were linked by CLs and a maximum pooling layer, as illustrated at the bottom of Figure 2. Dense connections were created to lessen the number of parameters necessary

in the network for high levels of throughput training while increasing interactions between network levels. After the dense blocks were processed, a “global average pooling” layer was used to determine the probability of a CL injury based on the compressed images which included the CL. The result of the classification was determined by averaging the probabilities of CL injury classification across all CL-containing image segments.

The suggested CNN was adapted from DenseNet, and it was compared to two other classification CNNs, one based on “Dense Deep Convolutional Networks for Large-Scale Image Recognition” and the other based on AlexNet, both of which have been applied to image classification applications in the past.

System for CL Injury Diagnosis Training and Evaluation

The CL injury diagnostic system evolved into an end-to-end autonomous system when the ThreeFoldCNNwas trained. For section-selection training CNN and the segregation of the ligament CNN, we first individually selected the MRI portions containing the CL and then manually delineated the precise position of the IN on the identified MRI sections. However, after training was finished, the CL injury diagnosis system allowed entirely computerized segregation of the CL on all MRI segments to be used as inputs into the categorization CNN. Participants with and without a surgical verified CL damage were split into "training, validation, and hold-out" testing groups randomly.

Iteratively optimizing the settings of the CNN allowed it to learn image features from a training dataset that included MRI from one hundred-six participants with an injury to their CL and 106 individuals with an intact CL. When selecting a suitable model to train on, we referred to the validation dataset, which included MRI from 26 participants with a CL injury and 25 subjects with an intact CL. The ideal model was finally assessed using the hold-out testing dataset, which included MRI from fifty individuals with a CL injury and 50 individuals with an intact CL. This was done to avoid excessive training fitting and confirm that the characteristics of the image acquired during training could be generalized to newly gathered image data.

SBO optimization

A cruciate ligament injury to the knee can be diagnosed and reconstructed with the use of a natural-inspired algorithm called Satin Bird Optimization. It optimizes diagnostics and treatments by emulating the mating behaviors of satin bowerbirds.

The Satin Bowerbird Optimizer (SBO) is a unique optimization system designed to mimic the natural mating habits of a male SB. The masculine SB increases the probability of a successful courting by creating a courting cabin, singing loudly and persistently to attract the opposite sex, and holding a glowing item in its beak. The male has double duty in protecting the nest from damage during courtship: he must ensure a prosperous courtship cabin is built, and he must also continually fend off challenges from other males. Based on the SB survival rules, the SBO algorithm consists of the following operations:

The first Satin Bowerbird population was generated at random. In a solution space, a random number of Naive Bayes (NB)individuals are formed as a starting population. The present population development algebra is s, and the precise spot of each courting cabin is defined as C-dimension.

An individual's probability of being selected is proportional to their fit value (objective function) as a fraction of the total fitness value. The probability of choosing the courting cabin is given by Equation (6), the value of the fitness of the jth courtship cabin is given by fit_j Equation (7), and the objective function value is given by $f(y_j)$.

$$Prob_j = \frac{fit_j}{\sum_{n=1}^{NC} fit_n} \tag{6}$$

$$fit_j = \begin{cases} \frac{1}{1+f(y_j)}, f(y_j) \geq 0 \\ 1 + \left| f\left(y_j\right) \right|, f\left(y_j\right) < 0 \end{cases} \tag{7}$$

The next step is to update the population data. Male SB is reported to iteratively refine the exact spot of their courting cabin depending on the information gathered from prior attempts. The current position formula is as follows:

$$y_{jl}^{s+1} = y_{jl}^{s} + \lambda_l \left(\left(y_{kl} + y_{elite,l} \right) - y_{jl}^{l} \right) \tag{8}$$

Where y_{jl}^{s} is the l -dimensional part of the jth person in the sth iteration; y_{kl} is the l -dimensional part of the best spot ever discovered at this time; y_l is chosen by the “roulette selection mechanism”; and $y_{elite,l}$ is

the l -dimensional part of the current global best spot for the entire population. The step factor is determined by equation (9) and is denoted byλ_l.

$$\lambda_l = \frac{\alpha}{1+Q_k} \tag{9}$$

Where Q_k is the probability of identifying the target courtship cabin, and is the maximal step size, and$Q_k \epsilon [0,1]$. Equation (9) makes it abundantly evident that the size of the step decreases as the probability of identifying the ideal spot increases. The biggest size in step, represented byα, occurs when there is no chance of choosing the destination position. The smallest step size, shown by the$\frac{\alpha}{2}$, occurs when the chance of choosing the destination location is 1.

Differentiation at the individual level prevents the phenomenon of "local optimization." It's very uncommon for an imposing male to rob and even demolish the courting huts of weaker guys. Therefore, the method incorporates a random mutation chance after each iteration to enhance the mutation over time. At this point, as illustrated by Equation (10), y_{jl} follows a normal distribution.

$$y_{jl}^{s+1} \sim N\left(y_{jl}^{s}, \sigma^2\right) \tag{10}$$

$$N\left(y_{jl}^{s}, \sigma^2\right) = y_{jl}^{s} + (\sigma * N(0,1)) \tag{11}$$

The calculation formula of the SD is as follows:

$$\sigma = a * (var_{max} - var_{min}) \tag{12}$$

Where $\mathrm{var}_{\max}$ and $\mathrm{var}_{\min}$ are the maximum and minimum values for variabley_j, a is the scaling factor.

At the end of each cycle, the original population and the mutated population are combined to produce a new combination population, and all of the individuals in the new population have their fitness values ranked from greatest to weakest. The most significant objective function value survives. If the last condition is met, the ideal position and value are outputted. Iteration will continue endlessly until the limit is reached.

This approach integrates Three-Fold Convolutional Neural Networks (ThreeFoldCNN) with Satin Bird Optimization, a nature-inspired approach recognized for its problem-solving effectiveness. The utilization of deep learning methods with ThreeFoldCNN improves the evaluation of medical imaging data, facilitating the identification of complex patterns and significant aspects that are essential for the diagnosis of CLdamages. This deep learning architecture is crucial in detecting small imperfections in medical images, therefore enhancing the accuracy of injury identification.

Satin Bird Optimization, which takes inspiration from the foraging habits of satin bowerbirds, enhances the reconstruction procedure by effectively exploring the solution area. This algorithm, inspired by biological processes, improves the preparation and execution of surgeries that reconstruct the CL, resulting in the best possible results for individuals.

The combination of ThreeFoldCNN with Satin Bird Optimization creates a synergistic strategy that improves both the accuracy of diagnosis and surgical treatment for CL injuries in the knee joint. This approach has the potential to greatly transform the area of orthopedics by offering a thorough and effective solution to the difficulties connected with these injuries.

Evaluation of CR

With the help of an image archiving and communication system (IACS), a "Fellowship-trained MR (FTMR) with thirteen years of clinical practice, an MR fellow (MRF), a 2nd-year radiology resident (RR 1), 3rd-year radiology resident (RR 2), and a 4th-year radiology resident (RR 3)"examined the MRI evaluations of all hundred individuals in the hold-out test dataset, allowing us to contrast the CL injury diagnosis system's diagnostic performance with that of clinical ratio. The five MRI sequences were merged by the CR, who was blind to the outcomes of the arthroscopic knee operations, to determine whether or not a CL injury had been made. Before examining the MRI data, the radiologists weren't involved in any formal training or calibration sessions.

Statistical Analysis

MATLAB and MedCalc were used for statistical analysis and the difference of $P < .05$ was considered to be significant. The sensitivity and specificity of the MRF, RR, suggested CL injury diagnosis technique and

MR, and a substitute CL injury diagnosis mechanisms with the classification CNNs adopted from VGG-16 were all measured against arthroscopic surgery in a "hold-out test dataset (HTD)" evaluation.

We examined the areas under the ROC curves (AUCs) of the proposed and other CL injury diagnostic approaches using a nonparametric technique termed "receiver operating characteristic (ROC)"analysis.

Maximum specificity and sensitivity for detecting CL injuries were calculated using the Youden index. The “confidence intervals-CIs” for the specificity and sensitivity of the suggested and other CL injury diagnosis methods and the CR, as well as the AUCs of the suggested and other CL injury diagnosis systems, were calculated using two-sided exact binomial testing. When the CR's point estimates of sensitivity and specificity for detecting injuries to the CL dropped beyond the 96% CIs of the AUC for the machine, it was considered to be statistically different from the machine's specificity and sensitivity.

RESULT AND DISCUSSION

CNNs for section selection required 0.82 hours to train, CNNs for ligament isolation required 5.11 hours, and CNNs for classification required 5.72 hours to train in the initial dataset for training. However, when employing the trained networks, the CL injury diagnosis method requires an average of 9 seconds to assess whether or not an individual has a CL injury.

To evaluate the occurrence or lack of a medically validated CL injury, Table 3 compares the recommended CL injury diagnostic system using the classification CNNs adapted from "VGG16 and AlexNet" with a different CL injury diagnosis system utilizing the categorization CNNs adopted from "DenseNet ."The estimated point values for specificity and sensitivity ranged between 0.89 and 0.97 and 0.90 and 0.97, respectively, while AUCs ranged from 0.91 to 98.5, indicating that all classification CNNs performed well. Figure 5 depicts the outcome for AUC, specificity, and sensitivity for the Suggested Method using CNN. The suggested CL injury diagnosis system, using a DenseNet-adapted classification CNN, outperformed all other methods in terms of overall diagnostic performance.

Table 3. Values for AUC, specificity, and sensitivity for the Suggested Method using CNN

CNN	AUC	Sensitivity	Specificity
Dense Net	98.5	97	97
Alex Net	91	90	89
VGG16	96	93	93

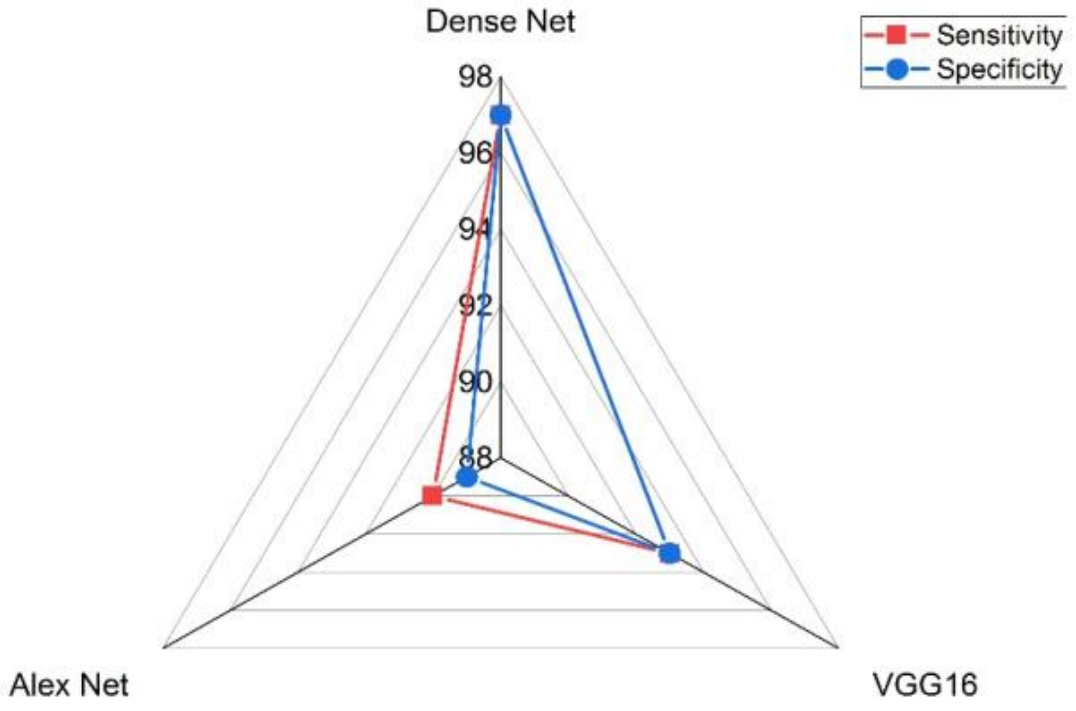

Figure 5. The outcome of specificity, and Sensitivity for the Suggested Method using CNN

Surgically verified CL injuries are shown in Table 4, while the specificity and sensitivity of the CR, MRF, RR, and the suggested CL injury diagnosis method are shown in Table 5 and Figure 6. At the ideal threshold of the “Youden index," the point estimates of the specificity and sensitivity of the suggested CL injury diagnosis system were 0.96 and 0.96, respectively.

Table 4. Values for the RR, MR, RF, and Proposed CL Injury Diagnosis System for the HTD

Reader and Result	Disease Present	Disease Absent	Total
CR			
Test positive	51	2	53
Test negative	2	51	53
Total	53	53	
R1			
Test positive	48	4	52
Test negative	5	49	54
Total	53	53	
MRF			
Test positive	49	3	52
Test negative	4	50	54
Total	53	53	
R2			
Test positive	49	3	52
Test negative	4	50	54
Total	53	53	
R3			
Test positive	50	3	53
Test negative	3	50	53
Total	53	53	
Machine			
Test positive	49	4	53
Test negative	4	49	53
Total	53	53	

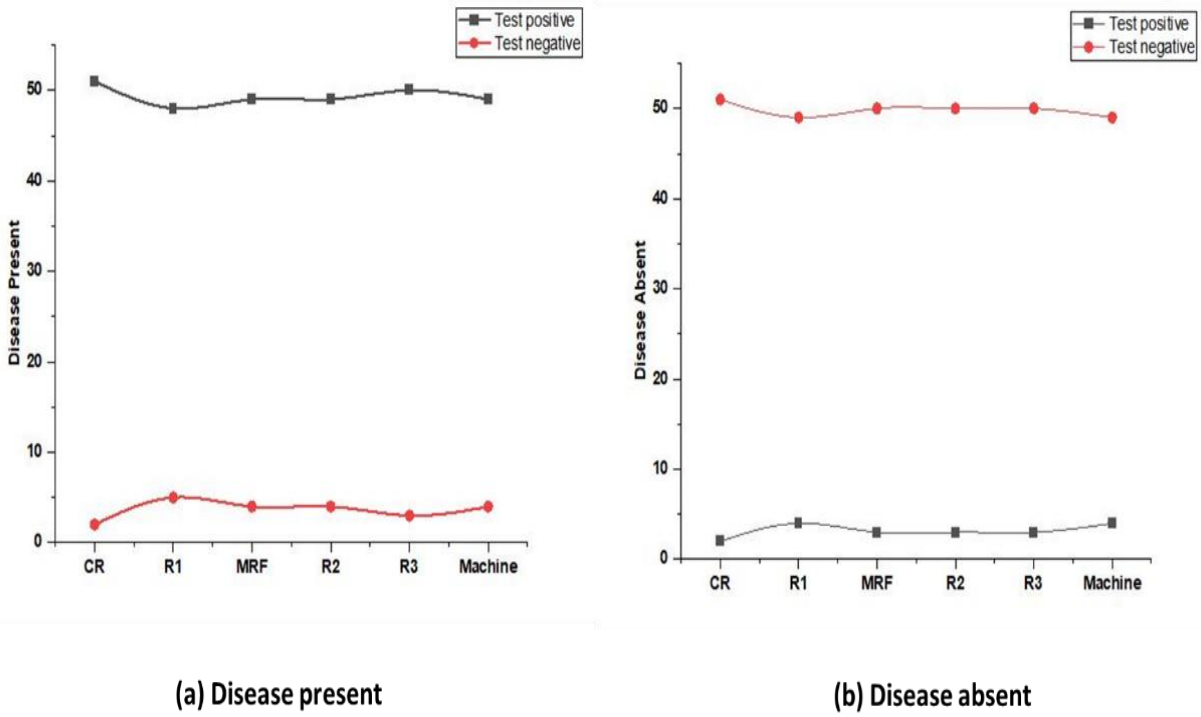

(a) Disease present (b) Disease absent

Figure 6. Outcome of RR, MR, RF, and Proposed CL Injury Diagnosis System for the HTD

Table 5. Specificity and sensitivity for CR, RR, MR, and suggested CL Injury Diagnosis System for the HTD

Reader	AUC	Sensitivity	Specificity
CR	98.5	98.5	98.5 (89,1)
MRF	98.5	97 (87,1)	98.5 (89,1)
R1	94	97 (87,1)	91 (79,98)
R2	97.5	97 (87,100)	98.5 (89,100)
R3	98.5	98.5 (89,1)	98.5 (89,1)
Machine	98.5	97 (90,1)	97 (87,1)

In contrast, the CR's point estimates of sensitivity ranged between 97 and 98.5, while their point estimates of specificity varied from 90.5 and 98.2. In particular, the fellowship-trained MR sensitivity and specificity point estimates were both 0.98.

Figure 7 depicts the ROC curve of the suggested CL tear detection system for detecting surgically demonstrated CL injury. The AUC value for CL injury detection was 98.5. The figure displays the ROC curve of the CL injury detection system, together with the value estimations representing the specificity and sensitivity of the MR, MRF, and RR in recognizing the presence or absence of a CL tear, allowing for comparison.All radiologists' sensitivity and specificity estimate points decreased within the 96% CIs of the AUC for the indicated CL injury diagnosis technique, with no significant variations among the CR and the machine.

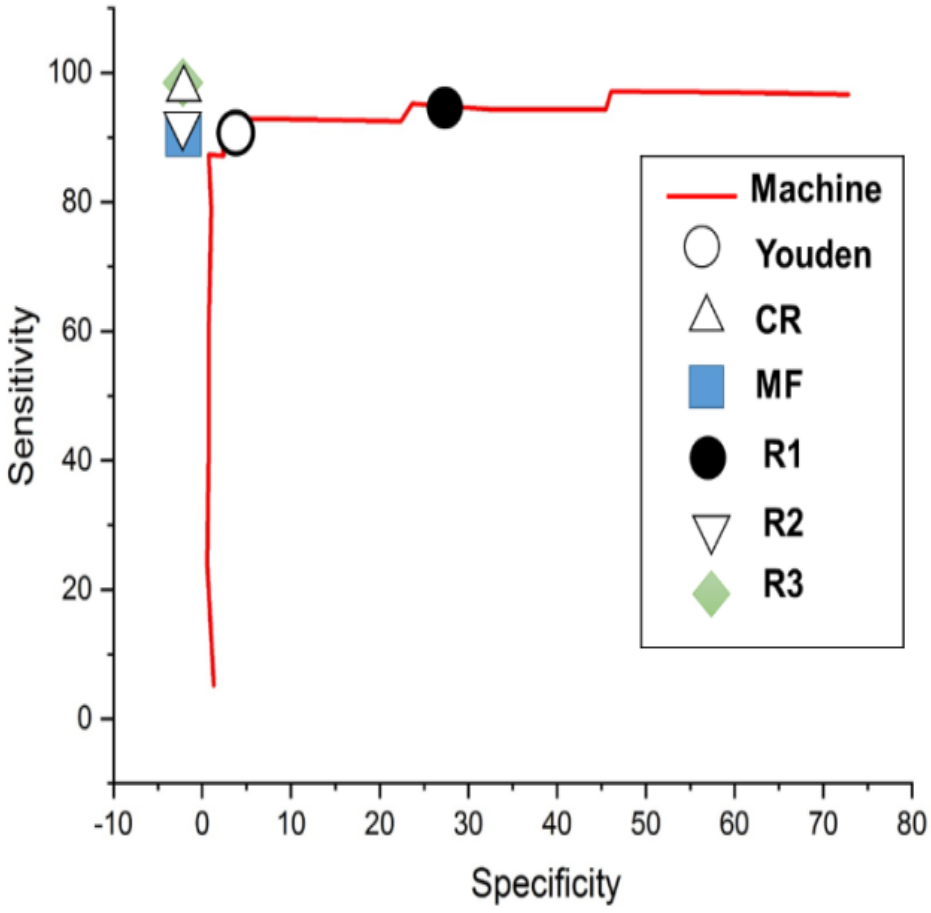

Figure 7. The outcome of the ROC curve

In this section, we also provide a performance comparison between the proposed method and existing techniques.The existing approaches such as U-Net, 2D-CNN and DCNN [21-23]. The comparison metrics are F1-score, precision, and accuracy.

Accuracy is determined by dividing the total number of cases studied by the percentage of true positive and true negative outcomes. True positives and true negatives are instances in which the model accurately recognizes the existence or absence of a CL injury, respectively. Figure 8 depicts the accuracy result. Our suggested ThreeFoldCNN+SBO is superior in diagnosing CL injury in knee joints when compared to the current approaches.

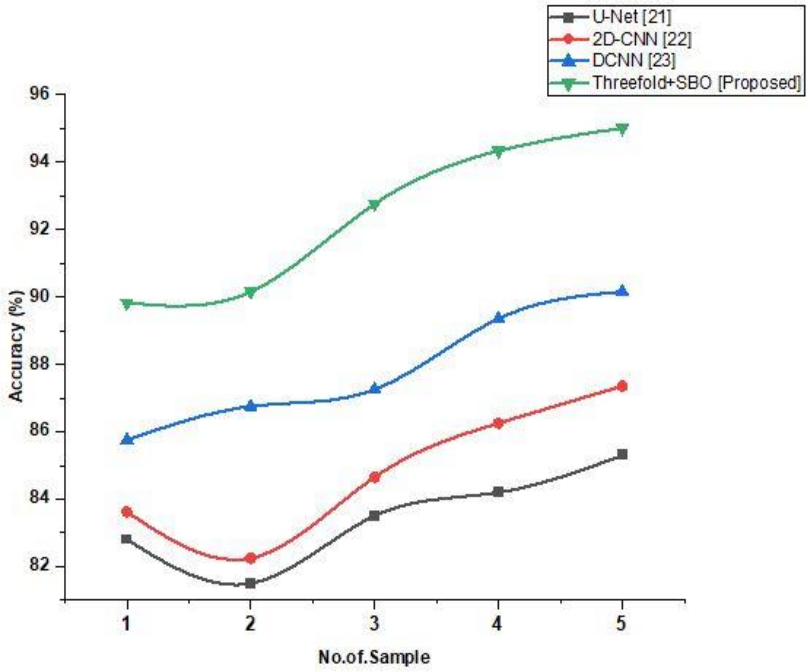

Figure 8. Accuracy result

Precision is employed to assess a classification model's effectiveness. Precision in the classification of cruciate ligament (CL) injuries of the knee joint is the percentage of true positives (i.e., properly classified CL injuries) among all the positive predictions produced by the model (i.e., all anticipated CL injuries) shown in Figure 9. In other words, precision assesses the efficacy of the model in predicting positive cases.When compared to the current methods, our ThreeFoldCNN+SBO is more effective at identifying CL injury in knee joints.

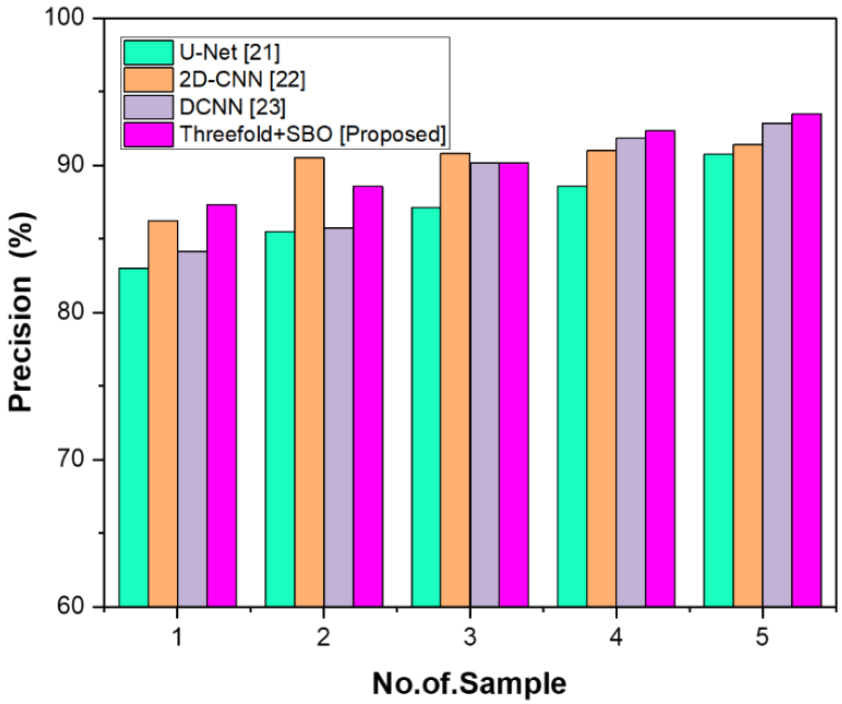

Figure 9. Precision result

A statistic for analyzing the effectiveness of a classification model is the F1 score. It calculates a single score that represents the model's performance by weighing precision and sensitivity. Our ThreeFoldCNN+SBO is more effective than the existing approaches in diagnosing CL injury in knee joints

when compared to others. Figure 10 depicts the f1-score result.The comparison output of accuracy, precision, and F1-score isshown in Table 6.

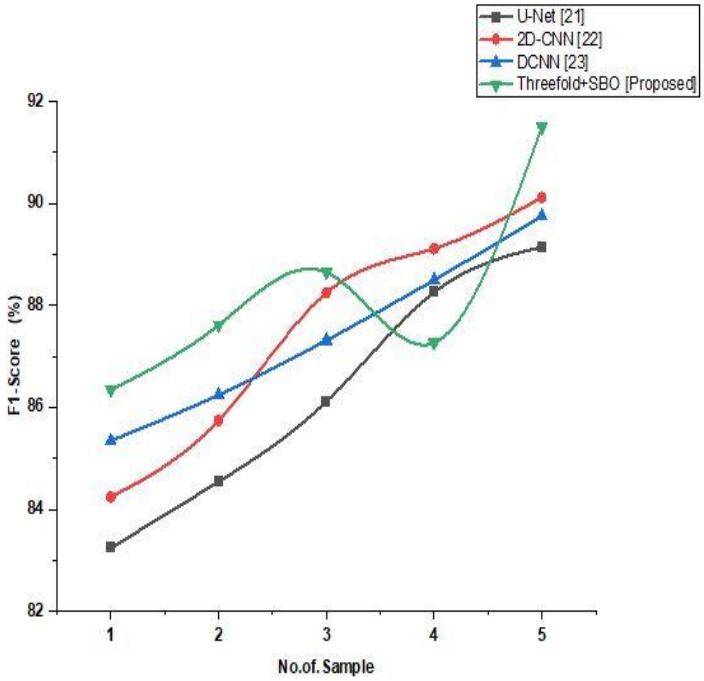

Figure 10. F1-score result

Table 6. Comparison output of accuracy, precision, F1-score

Methods	Accuracy (%)	Precision (%)	F1-score (%)
U-Net	85.3	90.75	89.15
2D-CNN	87.35	91.4	90.12
DCNN	90.15	92.85	89.75
Threefold+SBO [Proposed]	95	93.48	91.5

A computational cost graph that shows the relationship between the complexity of diagnostic and reconstructive operations and the necessary computational resources. It is used to show how cruciate ligament injuries in the knee joint can be diagnosed and repaired.Table 7 and Figure 11 depicts the outcome of computational cost. When comparing the proposed method(ThreeFoldCNN+SBO) (86.23) with the existing method U-Net (87.95) 2D-CNN (88.15) and DCNN (89.45) it shows that our suggested approach is better than the existing approach. This indicates that our proposed method is more effective.

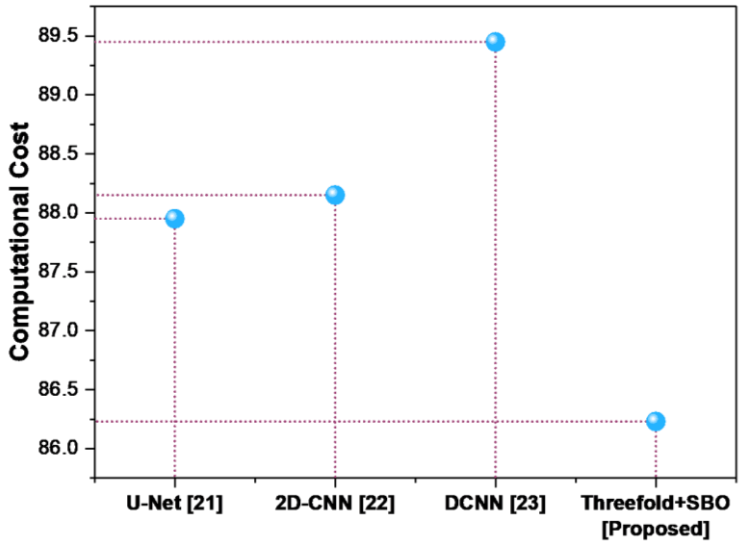

Figure 11. Computational cost

Table 7. The output of computational cost

Methods	U-Net	2D-CNN	DCNN	ThreeFoldCNN+SBO
Computational cost	87.95	88.15	89.45	86.23

Depending on the available technology, the severity of the injury, and the unique characteristics of the patient, the computational time required to diagnose and reconstruct cruciate ligament injuries of the knee can differ from several hours for assessment to several times for surgery preparation and performance.The comparison of computational time is presented in Figure 12 and Table 8.In comparison, the existing approachesU-Net (4.30sec) 2D-CNN (6.50sec), and DCNN (8.60sec), respectively, whereas our proposed approach has (2.40sec). According to the results, our suggested method is substantially lower than the existing approach.

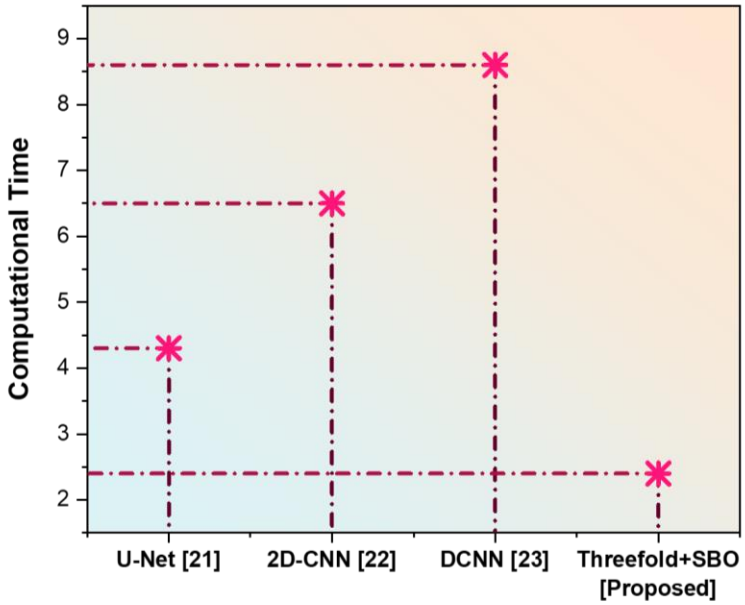

Figure 12. computational time

Table 8. Result of computational time

Methods	U-Net	2D-CNN	DCNN	ThreeFoldCNN+SBO
Computational Time	4.30sec	6.50sec	8.60sec	2.40sec

DISCUSSION

We found that a DL-based approach using arthroscopy as a reference standard can assess the complete thickness of CL injury in knee joints. With an AUC of 0.98, the CL injury detection technique demonstrated outstanding diagnostic performance for identifying a CL injury or not. Furthermore, the machine's sensitivity and specificity for identifying an injury to the CL did not differ statistically significantly from those of CR with different levels of expertise.The limitation of the CL injury diagnosis system was its ability to evaluate a small amount of "sagittal proton density-weighted and fat-suppressed T2-weighted fast spin-echo images". In contrast, the CR system was capable of evaluating every image section from a total of five separate MRIs.DenseNet, VGG16, and AlexNet were the threefold classifier CNNs that were the subject of our investigation, and we discovered that DenseNet had the greatest diagnostic accuracy for identifying an injury to the CL.The reason for AlexNet's more severe diagnostic performance was probably its fairly straightforward network design. The performance of the considerably more sophisticated VGG16 network may benefit from having enormous training datasets.DenseNet provides greater a connection compared to "AlexNet and VGG16" by utilizing a dense connection that facilitates direct information transmission across several network layers. This result in a reduction in the number of parameters needed to construct prediction

models.DenseNet's superior diagnostic accuracy on our miniature training dataset for CL injury detection was likely due to its dense connectivity. We also evaluate how well the proposed approach performs in comparison to the current methods. This demonstrates that the performance of our suggested strategy outperforms that of the alternatives.

Our study has several drawbacks. First, rather than being a single network from end to end, our DL-based CL injury detection system was made up of ThreeFoldCNN paired in a cascaded form. Because the ThreeFoldCNNwas trained separately, the training load could have increased.Our study also shows a drawback of a tiny training dataset. To this end, a combination of data processing methods, including transfer learning, was required to achieve optimal training effectiveness. In future research, it may be possible to significantly enhance the diagnostic performance of the CL injury detection system by using greater training datasets.

CONCLUSION

In this study, we offered a DL-based method (ThreeFoldCNN) for arthroscopically detecting injuries to the CL in the knee during MRI and to improve the model by using SBO. Our study has shown that arthroscopy is the best treatment and that a DL-based methodology may be utilized to identify a full-thickness CL lesion within the knee joint at MRI. Comparing the expertise levels of CR with the CL injury detection approach, we utilize sagittal proton density-weighted and fat-suppressed T2-weighted rapid spin-echo MRI to accurately evaluate whether a full-thickness CL injury is present or not. Until it can be used in clinical practice, the CL injury detection system still has to be technologically developed and validated. According to the outcomes, the CL destruction assessment system has a specificity of 97% and a sensitivity of 97%. The diagnostic physicians' specificity varied between 0.91% to 0.99%, while their sensitivity from 0.97% to 0.99%.Experimental result shows that our proposed method is better than the existing method in terms of Accuracy (95%), Precision (93.48%), f1-score (91.5%), computational cost(86.23%), and time(2.40sec).In particular, large prospective studies evaluating full- and partial-thickness CL injury subjects assessed with a variety of MRI units and imaging protocols are needed to better characterize the diagnostic performance of the CL injury detection system.

Funding: Shijiazhuang science and technology research and development plan: Clinical application of anchor and modified Krakow suture in reconstruction of fracture of knee extension device. (NO: 181460433).
Conflicts of Interest: The authors declare they have no conflicts of interest to report regarding the present study.

REFERENCES

1. Sahin MS. Midterm clinical outcomes of collateral ligament repair of the thumb and lesser digits: a retrospective analysis of 35 cases. BMC Musculoskelet.Disord.2022; 23(1):697.https://doi.org/10.1186/s12891-022-05605-1.
2. Ng JWG, Myint Y, Ali FM. Management of multiligament knee injuries. EFORT Open Rev. 2020 Mar 2;5(3):145-55. https://doi.org/10.1302%2F2058-5241.5.190012.
3. Anto A, Patil C. Effectiveness of Post-Isometric Relaxation Technique Versus Rhythmic Stabilization in Postoperative Anterior Cruciate Ligament Reconstruction. J. Coast. Life Med.2023; 11:1140-4.
4. Parameswari A, Bhavani S, Vinoth Kumar K. A Deep Learning Based Glioma Tumour Detection Using Efficient Visual Geometry Group Convolutional Neural Networks. Braz Arch Biol Technol. 2024;67:e24230705. https://doi.org/10.1590/1678-4324-2024230705
5. Tang C, Kwaees TA, Accadbled F, Turati M, Green DW, Nicolaou N. Surgical techniques in the management of pediatric anterior cruciate ligament tears: Current concepts.J.Child'sOrthop.2023 Feb;17(1):12-21. https://doi.org/10.1177/18632521221149059.
6. Kerzner B, Swindell HW, Terhune EB, Ramos P, Fortier LM, Dasari SP, et al. Medial Collateral Ligament and Posterior Oblique Ligament Reconstruction for Valgus Instability After Total Knee Arthroplasty. Arthrosc. Tech. 2022 Aug;11(9):e1531-9. https://doi.org/10.1016/j.eats.2022.04.003.
7. Chen J,Chen Y.Nanoligament Combined with Tennis Exercise on Rehabilitation Training for Treatment of Ligament Injury Patients. J. Nanomater. 2022; https://doi.org/10.1155/2022/1575200.
8. Zhang S,Lv Z. Diagnosis and exercise rehabilitation of knee joint anterior cruciate ligament injury based on 3D-CT reconstruction. Complex. 2020; 1-13. https://doi.org/10.1155/2020/3690124
9. Chang PD, Wong TT,Rasiej MJ. Deep learning for detection of complete anterior cruciate ligament tear. J. Digit. Imaging. 2019; 32:980-6.https://doi.org/10.1007/s10278-019-00193-4.
10. Chaudhari AS, Grissom MJ, Fang Z, Sveinsson B, Lee JH, Gold GE, et al. Diagnostic accuracy of quantitative multicontrast 5-minute knee MRI using prospective artificial intelligence image quality enhancement. Am. J. Roentgenol.. 2021; 216(6):1614-25.https://doi.org/10.2214/ajr.20.24172.

11. Parameswari A, Bhavani S, Vinoth Kumar K. A Convolutional Deep Neural Network Based Brain Tumor Diagnoses Using Clustered Image and Feature-Supported Classifier (CIFC) Technique. Braz Arch Biol Technol. 2023;66:e23230012. https://doi.org/10.1590/1678-4324-2023230012
12. Dung NT, Thuan NH, Van Dung T, Van Nho L, Tri NM, Vy VPT, et al. End-to-end deep learning model for segmentation and severity staging of anterior cruciate ligament injuries from MRI.Diagn.Interv.Imaging.2023; 104(3):133-141.https://doi.org/10.1016/j.diii.2022.10.010.
13. Parameswari A, Vinoth Kumar K, Gopinath S. Thermal analysis of Alzheimer's disease prediction using Random Forest Classification Model. Mater Today Proc. 2022;66(3). https://doi.org/10.1016/j.matpr.2022.04.357
14. Kakigi T, Sakamoto R, Tagawa H, Kuriyama S, Goto Y, Nambu M, et al. Diagnostic advantage of thin slice 2D MRI and multi-planar reconstruction of the knee joint using deep learning based denoising approach. Sci.Rep.2022; 12(1):1-14. https://doi.org/10.1038/s41598-022-14190-1.
15. Stephe S, JayaSankar T, Vinoth Kumar K. Motor imagery recognition of EEG signal using cuckoo-search masking empirical mode decomposition. Int J Innov Technol Explor Eng. 2019;8(11). https://doi.org/10.35940/ijitee.K2175.0981119.
16. Siouras A, Moustakidis S, Giannakidis A, Chalatsis G, Liampas I, Vlychou M, et al. Knee Injury Detection Using Deep Learning on MRI Studies: A Systematic Review. Diagnostics. 2022 Feb;12(2):537. https://doi.org/10.3390%2Fdiagnostics12020537.
17. Namiri NK, Flament I, Astuto B, Shah R, Tibrewala R, Caliva Fet al.Deep Learning for Hierarchical Severity Staging of Anterior Cruciate Ligament Injuries from MRI. RadiolArtifIntell. 2020 Jul; 2(4):e190207. doi: 10.1148/ryai.2020190207. https://doi.org/10.1148/ryai.2020190207.
18. Javed Awan M, ShafryMohd Rahim M, Salim N, Rehman A, Nobanee H, Shabir H. Improved Deep Convolutional Neural Network to Classify Osteoarthritis from Anterior Cruciate Ligament Tear Using Magnetic Resonance Imaging. J Pers Med. 2021 Nov;11(11):1163. https://doi.org/10.3390/jpm11111163.
19. Jayanthi J, Jayasankar T, Krishnaraj N, Prakash NB, Britto ASF, Vinoth Kumar K. An Intelligent Particle Swarm Optimization with Convolutional Neural Network for Diabetic Retinopathy Classification Model. J Med Imaging Health Inform. 2021;11(3):803-9.
20. Pedoia V, Norman B, Mehany SN, Bucknor MD, Link TM, Majumdar S. 3D convolutional neural networks for detection and severity staging of meniscus and PFJ cartilage morphological degenerative changes in osteoarthritis and anterior cruciate ligament subjects.J.Magn.Reson.Imaging.2019; 49(2):400-10.https://doi.org/10.1002/jmri.26246.
21. Namiri NK, Flament I, Astuto B, Shah R, Tibrewala R, Caliva F, et al.Deep Learning for Hierarchical Severity Staging of Anterior Cruciate Ligament Injuries from MRI. RadiolArtifIntell. 2020 Jul 29;2(4):e190207.https://doi.org/10.1148%2Fryai.2020190207.
22. Stephe S, Jaya Sankar T, Vinoth Kumar K. Motor Imagery EEG Recognition using Deep Generative Adversarial Network with EMD for BCI Applications. Tehnički vjesnik. 2022;29(1). https://doi.org/10.17559/TV-20210121112228
23. Germann C, Marbach G, Civardi F, Fucentese SF, Fritz J, Sutter R, et al. Deep Convolutional Neural Network-Based Diagnosis of Anterior Cruciate Ligament Tears: Performance Comparison of Homogenous Versus Heterogeneous Knee MRI Cohorts with Different Pulse Sequence Protocols and 1.5-T and 3-T Magnetic Field Strengths. Invest Radiol. 2020 Aug; 55(8):499-506. https://doi.org/10.1097/rli.0000000000000664.